J. Fluid Mech. (1983), *vol.* 135, *pp.* 219–233
Printed in Great Britain

Numerical calculations of two-cell and single-cell Taylor flows

By K. A. CLIFFE
Theoretical Physics Division, AERE Harwell, Didcot, Oxon OX11 0RA

(Received 21 February 1983)

Numerical solutions of the Navier–Stokes equations for steady axisymmetric flow in the Taylor experiment are presented. In the cases considered the annulus is so short that only one or two Taylor cells are present. The results are compared with a recent theoretical and experimental study by Benjamin & Mullin (1981). The qualitative picture of the flows possible proposed by Benjamin & Mullin is confirmed by the calculations, and the quantitative agreement with their experimental results is quite satisfactory.

1. Introduction

This paper is concerned with the flow in a Taylor apparatus where the length of the annulus is comparable to the difference between the outer and inner radii. All the flows considered have only one or two Taylor cells. Needless to say, the effect of the ends of the annulus is very important in this case. Consequently little help towards understanding these flows is given by most of the standard theory about the Taylor experiment (e.g. DiPrima 1981), in which theory the cylinders are assumed to be infinitely long.

Schaeffer (1980) has analysed a model for boundary effects in the Taylor problem. His analysis was qualitative and he was primarily concerned with phenomena such as observed by Benjamin (1978*b*) and by Mullin (1982) which depend on the way in which the number of cells present in the primary flow changes as the length of the cylinders increases. The primary flow may be defined as that produced by slowly increasing the speed of the inner cylinder from rest; all other flows are called secondary modes. Although Schaeffer did not consider the present case, his model is relevant, and Benjamin & Mullin (1981) have already used it, together with a general theory of bifurcation phenomena in steady viscous-fluid flow developed by Benjamin (1976, 1978*a*, *c*), to interpret their experimental observations. They have given a reasonably complete qualitative account of the flows possible when the cylinders are very short.

The purpose of this paper is to present numerical solutions of the Navier–Stokes equations for steady axisymmetric flow in the Taylor experiment when the cylinders are so short that only one or two Taylor cells are present. The results are compared with those obtained experimentally by Benjamin & Mullin (1981), and in view of the delicacy of the experiments one appreciates the quantitative agreement to be quite satisfactory. More importantly, precisely the same qualitative picture as that proposed by Benjamin & Mullin (1981) emerges from the numerical calculations. In particular, the general theory makes predictions about unstable flows, which cannot of course be observed but which are confirmed by the numerical results.

The numerical approach adopted is to discretize the appropriate boundary-value

problem by the finite-element method and then to apply the methods of bifurcation theory to obtain multiple solutions of the equations as the Reynolds number and aspect ratio are varied. It should be stressed that separate solutions sometimes occur in close proximity and that a naive approach to the problem will at best be highly inefficient.

In §2 the Benjamin theory will be summarized. The numerical methods will be described in §3, and the results obtained will be presented in §4. Finally, some conclusions are drawn in §5.

2. General theory

We summarize here the general theory of bifurcation in steady viscous-fluid flow that was developed by Benjamin and specifically applied to single-cell flows by Benjamin & Mullin (1981). The theory applies to the Navier–Stokes equations in any bounded domain, and is concerned with the qualitative properties of the solution set as the Reynolds number R is varied. It is important to notice that this theory can also be applied to the finite-element discretization of the Navier–Stokes equations considered in this paper. (With non-homogeneous boundary conditions, however, some of the results apply only when the mesh is sufficiently fine.) Further, the Leray–Schauder index of a solution, as noted below, can be obtained as part of the solution procedure. This considerably simplifies the interpretation of the numerical results in terms of the general theory. Section 3 contains more details on this point.

Let X denote the function space in which the solutions lie and $S(R)$ the set of solutions of the Navier–Stokes equations, with appropriate boundary conditions, when the Reynolds number is R. The main theoretical conclusions are as follows.

(i) For any positive value of the Reynolds number R there is at least one solution of the steady Navier–Stokes equations (cf. Ladyzhenskaya 1969). For sufficiently small values of R this solution is unique and globally stable (Serrin 1959); any initial velocity field evolves towards the unique steady solution as time increases.

(ii) A generic property of the solution set $S(R)$ is that its members are isolated in X for a particular value of R (Foias & Temam 1977). This implies that there is a finite number of solutions. Only under very special conditions it is possible to have a continuum of solutions (for more details see Benjamin 1978*c*).

(iii) Except at singular points at which the number of solutions changes (e.g. bifurcation or turning points), each member of $S(R)$ has an index i equal to 1 or -1 (the Leray–Schauder index). As R varies, i remains constant along a solution branch unless such a singular point is reached. With the same qualification, the index i is also constant with respect to changes in the domain and boundary data.

(iv) For a given R, label the solutions by $m = 1, 2, \ldots, k$. Then

$$\sum_{m=1}^{k} i_m = 1.$$

Together with (iii) this implies that there is an odd number of solutions for any value of R for which the solution set $S(R)$ contains no singular points.

(v) Any solution with $i = -1$ not at a singular point represents an unstable steady flow (Benjamin 1976, theorem 3).

We turn now to the Taylor experiment with symmetric end conditions. We use cylindrical polar coordinates (r, ϕ, z) with origin midway between the ends. The

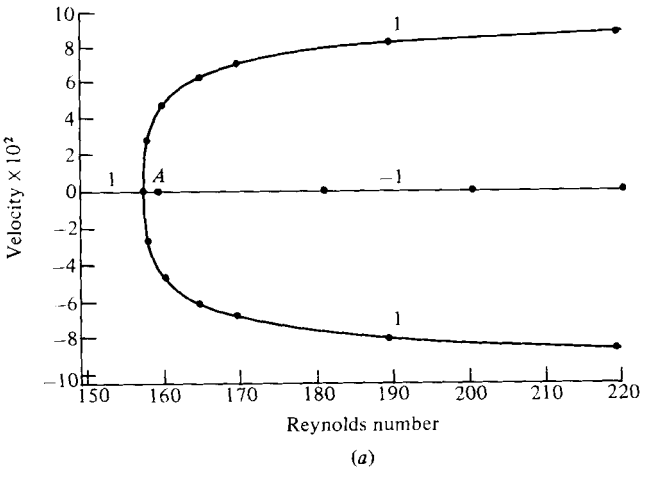

(*a*)

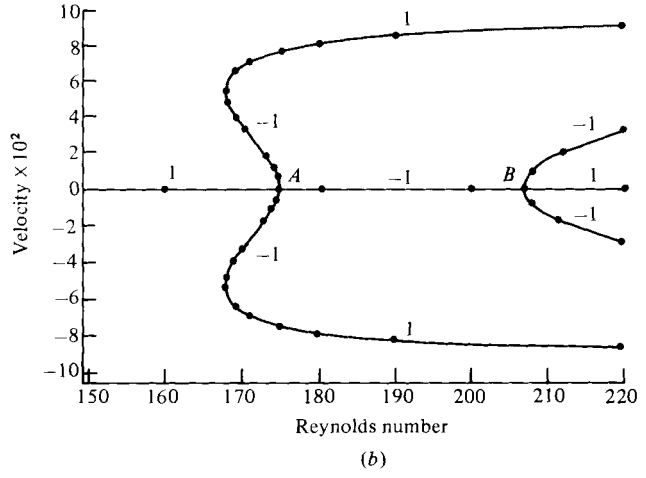

(*b*)

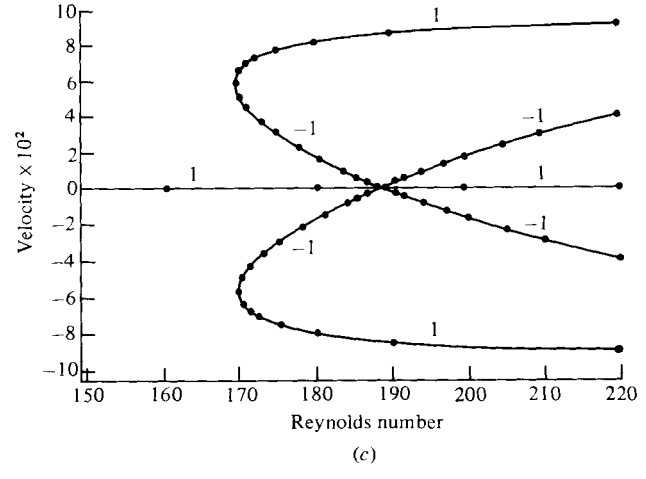

(*c*)

FIGURE 1. For caption see p. 222.

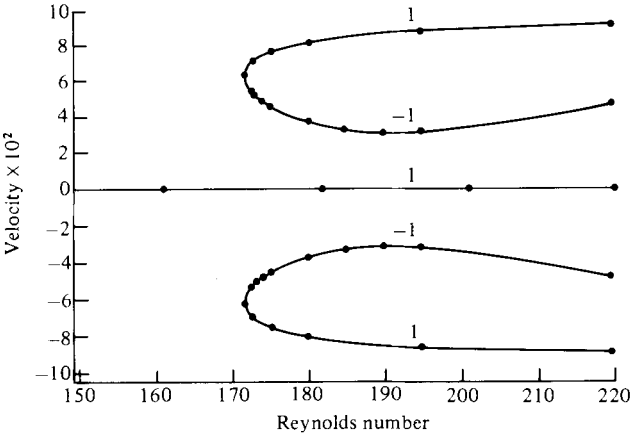

FIGURE 1. Numerically calculated state diagrams. The vertical velocity at point (0.75, 0) is plotted against Reynolds number for various aspect ratios; the dots indicate the calculated points. (*a*) $\Gamma = 1.23$, (*b*) 1.26, (*c*) 1.264, (*d*) 1.27. Cf. Benjamin & Mullin (1981, figure 6).

corresponding velocity components are (u_r, u_ϕ, u_z). Following Benjamin (1978*b*) we recognize two classes of symmetry:

class (i): (u_r, u_ϕ, u_z) = (even, even, odd) function of z;

class (ii): (u_r, u_ϕ, u_z) = (odd, odd, even) function of z.

It is easy to see that the primary flow, as defined in the second paragraph, belongs to class (i). Also any solution may be written in the form $\boldsymbol{U}_1 + \boldsymbol{U}_2$, where $\boldsymbol{U}_1$ is a member of class (i) and $\boldsymbol{U}_2$ a member of class (ii). Further, if $\boldsymbol{U}_1 + \boldsymbol{U}_2$ is a solution, then so is $\boldsymbol{U}_1 - \boldsymbol{U}_2$. A simple consequence is that solutions either have streamline patterns which are symmetric about the mid-plane or else they occur in asymmetric pairs. Under these conditions a supercritical bifurcation is possible (cf. Werner & Spence 1983; Brezzi, Rappaz & Raviart 1981*b*). The most common form of bifurcation is the simple turning point or one-sided bifurcation. If two-sided bifurcations occur then they are typically transcritical or asymmetric (Benjamin 1976).

We can now outline the qualitative picture of the flows possible when the cylinders are short, proposed by Benjamin & Mullin (1981). For sufficiently short cylinders there is a stable primary flow which belongs to symmetry class (i) and has two Taylor cells. At a critical value R_1 of R, there is a supercritical bifurcation into a pair of single-cell flows. The two-cell flow exchanges stability with the single-cell flows in the usual fashion. A stable two-cell flow also exists for sufficiently large values of R, but loses stability as R is reduced to a second critical value R_2 ($> R_1$).

At larger cylinder lengths the single-cell flow becomes a genuine secondary mode in the sense that it is disconnected from the primary branch of solutions and cannot be generated by slowly increasing the speed of the inner cylinder. In this case the primary two-cell flow does not undergo a bifurcation.

The sequence of events leading to this change in the structure of the solution is shown in figure 1. In practice the change occurs over a very short range of cylinder lengths. Benjamin & Mullin (1981) found that an increase of about 8% in the length covered the changes shown in figure 1. As the length of the cylinders is increased the two bifurcations at A and B move closer together. The bifurcation at A becomes

subcritical, so giving rise to hysteresis effects, and eventually coalesces with the one at B at an aspect ratio slightly greater than that of figure 1 (*c*). The two bifurcating branches join together and separate from the primary flow as shown in figure 1 (*d*). The values of the Leray–Schauder index associated with each of the solution branches are also shown in figure 1. Note again that solutions with index -1 represent unstable steady flows which cannot be observed.

Benjamin & Mullin (1981) determined the loci of the various bifurcation points shown in figure 1, in the Reynolds-number/aspect-ratio plane. These points were determined by flow-visualization techiques, being the limiting values of Reynolds number for which a particular flow remains stable at a given aspect ratio.

3. Governing equations and numerical methods

Let r_1 and r_2 be the radii of the inner and outer cylinders respectively and let l be their length. Let Ω be the angular speed of the inner cylinder, the outer cylinder being taken to be stationary. We use cylindrical polar coordinates (r^*, ϕ, z^*) with the origin midway between the ends and denote the velocity by $\boldsymbol{U}^* \equiv (u_r^*, u_\phi^*, u_z^*)$. The equations for axisymmetric flow of a viscous fluid are

$$R\left(\Gamma u_r \frac{\partial u_r}{\partial r} + u_z \frac{\partial u_r}{\partial z} - \frac{\Gamma u_\phi^2}{r+\beta}\right) + \Gamma \frac{\partial p}{\partial r} - \frac{\Gamma}{r+\beta}\frac{\partial}{\partial r} 2(r+\beta)\frac{\partial u_r}{\partial r} - \frac{\partial}{\partial z}\left(\frac{1}{\Gamma}\frac{\partial u_r}{\partial z} + \frac{\partial u_z}{\partial r}\right) + \frac{\Gamma u_r}{(r+\beta)^2} = 0, \quad (3.1)$$

$$R\left(\Gamma u_r \frac{\partial u_\phi}{\partial r} + u_z \frac{\partial u_\phi}{\partial z} + \Gamma \frac{u_r u_\phi}{r+\beta}\right) - \frac{\Gamma}{r+\beta}\frac{\partial}{\partial r}(r+\beta)\frac{\partial u_\phi}{\partial r} - \frac{1}{\Gamma}\frac{\partial^2 u_\phi}{\partial z^2} + \Gamma \frac{u_\phi}{(r+\beta)^2} = 0, \quad (3.2)$$

$$R\left(\Gamma u_r \frac{\partial u_z}{\partial r} + u_z \frac{\partial u_z}{\partial z}\right) + \frac{\partial p}{\partial z} - \frac{1}{r+\beta}\frac{\partial}{\partial r}(r+\beta)\left(\Gamma \frac{\partial u_z}{\partial r} + \frac{\partial u_r}{\partial z}\right) - \frac{2}{\Gamma}\frac{\partial^2 u_z}{\partial z^2} = 0, \quad (3.3)$$

$$\frac{\Gamma}{r+\beta}\frac{\partial}{\partial r}(r+\beta)\, u_r + \frac{\partial u_z}{\partial z} = 0. \quad (3.4)$$

In the above equations r, z, $\boldsymbol{U}$ and p are given by

$$z = \frac{z^*}{l}, \quad r = \frac{r^*}{d} - \beta, \quad \boldsymbol{U} = \frac{\boldsymbol{U}^*}{r_1 \Omega}, \quad p = \frac{dp^*}{\mu r_1 \Omega},$$

where $d = r_2 - r_1$ and $\beta = r_1/d$. The aspect ratio $\Gamma = l/d$ and the Reynolds number $R = \rho r_1 \Omega d/\mu$, where ρ and μ are the fluid density and viscosity respectively. Thus the problem has one dynamical parameter R and two geometrical parameters Γ and β.

It is more usual to take the second geometrical parameter as the radius ratio $\eta = r_1/r_2 = \beta/(1+\beta)$.

Equations (3.1)–(3.4) hold in the region

$$D = \{(r, z) | 0 \leqslant r \leqslant 1, -0.5 \leqslant z \leqslant 0.5\}. \quad (3.5)$$

The boundary conditions are that u_r and u_z are zero on the entire boundary of D, and that u_ϕ is zero on the outer cylinder and 1 on the inner cylinder. The simplest condition on the ends would be to impose $u_\phi = 0$. However, this implies a discontinuity in this component of velocity, which in turn implies an infinite rate of dissipation in a Newtonian fluid. Further, in any experiment the azimuthal velocity clearly

cannot have a discontinuity though the exact form it takes would be very difficult to determine. Fortunately the numerical results indicate that the exact form of this boundary condition only affects the flow locally (see §4) and so we assume that the azimuthal velocity on the ends increases from zero to one, at the inner cylinder, over a short distance ϵ. A more complete discussion of this point is given by Benjamin & Mullin (1981).

The starting point for a finite-element discretization of (3.1)–(3.4) is an integral formulation of the problem. We introduce the following notation: let $L^2(D)$ be the space of functions that are square-integrable over D; let $W^{1,2}(D)$ be the space of functions whose generalized first derivatives lie in $L^2(D)$, and let $W_0^{1,2}(D)$ be that subspace of $W^{1,2}(D)$ whose elements vanish (weakly) on the boundary of D. $W^{1,2}(D)^3$ is the space of vector-valued functions each component of which is in $W^{1,2}(D)$.

We introduce the following three functionals:

$$a_1(\boldsymbol{U};\boldsymbol{V},\boldsymbol{W}) = R\int_D \Big[\Big\{(r+\beta)\Big(\Gamma u_r\frac{\partial v_r}{\partial r}+u_z\frac{\partial v_r}{\partial z}\Big)-\Gamma u_\phi v_\phi\Big\}w_r + \Big\{(r+\beta)\Big(\Gamma u_r\frac{\partial v_\phi}{\partial r}+u_z\frac{\partial v_\phi}{\partial z}\Big)+\Gamma u_r v_\phi\Big\}w_\phi + (r+\beta)\Big\{\Gamma u_r\frac{\partial v_z}{\partial r}+u_z\frac{\partial v_z}{\partial z}\Big\}w_z\Big], \tag{3.6}$$

$$a_0(\boldsymbol{U},\boldsymbol{V}) = \int_D \Big[2\Gamma(r+\beta)\frac{\partial u_r}{\partial r}\frac{\partial v_r}{\partial r}+(r+\beta)\Big(\frac{1}{\Gamma}\frac{\partial u_r}{\partial z}+\frac{\partial u_z}{\partial r}\Big)\frac{\partial v_r}{\partial z} + \frac{\Gamma u_r v_r}{r+\beta}+\Gamma(r+\beta)\frac{\partial u_\phi}{\partial r}\frac{\partial v_\phi}{\partial r}+\frac{r+\beta}{\Gamma}\frac{\partial u_\phi}{\partial z}\frac{\partial v_\phi}{\partial z} + \Gamma\frac{u_\phi v_\phi}{r+\beta}+(r+\beta)\Big(\Gamma\frac{\partial u_z}{\partial r}+\frac{\partial u_r}{\partial z}\Big)\frac{\partial \sigma_z}{\partial r}+2\frac{r+\beta}{\Gamma}\frac{\partial u_z}{\partial z}\frac{\partial v_z}{\partial z}\Big], \tag{3.7}$$

$$b(q,\boldsymbol{V}) = -\int_D\Big[\Gamma q\frac{\partial}{\partial r}(r+\beta)v_r+q(r+\beta)\frac{\partial v_z}{\partial z}\Big]. \tag{3.8}$$

Let $\hat{\boldsymbol{U}}\in W^{1,2}(D)^3$ be a vector-valued function that satisfies the boundary conditions of the problem. We can now state the appropriate integral form:

Find $\boldsymbol{U}\in W^{1,2}(D)^3$, $p\in L^2(D)$ such that

$$\text{(i)}\quad \boldsymbol{U}-\hat{\boldsymbol{U}}\in W_0^{1,2}(D)^3, \tag{3.9}$$

$$\text{(ii)}\quad a_1(\boldsymbol{U};\boldsymbol{U},\boldsymbol{V})+a_0(\boldsymbol{U},\boldsymbol{V})+b(p,\boldsymbol{V})=0 \quad \text{for all} \quad \boldsymbol{V}\in W_0^{1,2}(D)^3, \tag{3.10}$$

$$\text{(iii)}\quad b(q,\boldsymbol{U})=0 \quad \text{for all} \quad q\in L^2(D). \tag{3.11}$$

For each h let W_h and M_h be two finite-dimensional spaces such that $W_h\subset W^{1,2}(D)^3$, $M_h\subset L^2(D)$; and let $W_{h,0}=W_h\cap W_0^{1,2}(D)^3$.

Let $\hat{\boldsymbol{U}}_h\in W_h$ be a vector-valued function that approximates the boundary conditions of the problem and satisfies $b(1,\hat{\boldsymbol{U}}_h)=0$. The finite-element approximation of (3.9)–(3.11) is simply to find $\boldsymbol{U}_h\in W_h$, $p_h\in M_h$ such that

$$\text{(i)}\quad \boldsymbol{U}_h-\hat{\boldsymbol{U}}_h\in W_{h,0}, \tag{3.12}$$

$$\text{(ii)}\quad a_1(\boldsymbol{U}_h;\boldsymbol{U}_h,\boldsymbol{V}_h)+a_0(\boldsymbol{U}_h,\boldsymbol{V}_h)+b(p_h,\boldsymbol{V}_h)=0 \quad \text{for all} \quad \boldsymbol{V}_h\in W_{h,0}, \tag{3.13}$$

$$\text{(iii)}\quad b(q_h,\boldsymbol{U}_h)=0 \quad \text{for all} \quad q_h\in M_h. \tag{3.14}$$

The space W_h is generated by nine-node isoparametric quadrilateral elements with biquadratic interpolation. The space M_h is generated by piecewise linear interpolation

on the same elements, the interpolation being, in general, discontinuous across element boundaries. The parameter h is the length of the longest edge in the mesh. Examples of the use of this element can be found in Engleman *et al.* (1982) and Cliffe, Jackson & Greenfield (1982).

Equations (3.13) and (3.14) form a set of nonlinear equations for the parameters specifying the velocity and pressure. They depend on three scalar parameters R, Γ and β. Before describing the methods used to solve the equations we summarize their theoretical properties. These results are taken from Girault & Raviart (1979) and Brezzi, Rappaz & Raviart (1980, 1981*a*, *b*).

If $(\boldsymbol{U}, p)$ is a solution of the Navier–Stokes equations away from a bifurcation point, the following error estimates hold:

$$\|\boldsymbol{U}-\boldsymbol{U}_h\|_1 < C_1 h^2, \tag{3.15}$$

$$\|p-p_h\|_0 < C_2 h^2. \tag{3.16}$$

(Here norms for $W^{1,2}$ and L^2 are denoted by subscripts 1 and 0 respectively.)

If for given Γ and β, (3.1)–(3.4) have a simple limit point (one-sided bifurcation) at $(\boldsymbol{U}_0, p_0, R_0)$, then the discrete equations (3.13) and (3.14) also have a simple limit point at $(\boldsymbol{U}_{h,0}, p_{h,0}, R_{h,0})$, which is close to $(\boldsymbol{U}_0, p_0, R_0)$. The following error estimates hold:

$$\|\boldsymbol{U}_0-\boldsymbol{U}_{h,0}\|_1 < C_3 h^2, \tag{3.17}$$

$$\|p_0-p_{h,0}\|_0 < C_4 h^2, \tag{3.18}$$

$$|R_0-R_{h,0}| < C_5 h^4. \tag{3.19}$$

It is worth emphasizing the high order of convergence of the critical Reynolds number as the mesh is refined.

In general, a numerical approximation to a problem having a two-sided bifurcation need not also have bifurcation. However, in the special case of a symmetry-breaking bifurcation, the discrete problem also bifurcates (Brezzi *et al.* 1981*b*) and precisely the same error estimates may be established as for the simple limit point.

We turn now to the methods used to solve equations (3.13) and (3.14). For convenience we denote the pair $(\boldsymbol{U}_h, p_h)$ by $\mathscr{U}$ and the equations by

$$\boldsymbol{g}(\mathscr{U}, R, \Gamma, \beta) = 0. \tag{3.20}$$

A complete solution for axisymmetric flow in the Taylor problem consists of all $\mathscr{U}$ that satisfy (3.20) for some values of R, Γ and β. Note that we cannot say $\mathscr{U}$ is a function of (R, Γ, β) since, in general, there is more than one $\mathscr{U}$ satisfying (3.20), for each (R, Γ, β). The work of Benjamin (1978*b*), Benjamin & Mullin (1981, 1982) and Mullin (1982) has shown that the solution set becomes progressively more complex as R and Γ increase. Moreover, their work did not include a study of the effect of variations of β (or η). It is clear, therefore, that even the restricted case of steady axisymmetric flow in the Taylor experiment poses a very formidable numerical problem. In this paper we restrict our attention to the case where β is fixed, $\beta = 1.597$ ($\eta = 0.615$), and $0.6 \leqslant \Gamma \leqslant 1.51$.

For the rest of the paper, β will always have the value 1.597 and so we drop it from (3.20). If we also fix Γ, then (3.20) is an equation with a single scalar parameter. Further, we know that for small values of R the solution is unique (§2, point (i)). Newton's method can be used to solve the equations under these conditions, and then Euler–Newton continuation can be used to trace out the behaviour as R is increased. Newton's method defines the following iterates $\mathscr{U}^n$:

$$\frac{\partial \boldsymbol{g}}{\partial \mathscr{U}}(\mathscr{U}^n, R)\,(\mathscr{U}^{n+1}-\mathscr{U}^n) = -\boldsymbol{g}(\mathscr{U}^n, R). \tag{3.21}$$

The continuation procedure provides a good initial guess for the next value of R, i.e.

$$\mathscr{U}(R+\delta R) = \mathscr{U}(R) + \frac{\partial \mathscr{U}}{\partial R}\delta R, \tag{3.22}$$

$$\frac{\partial \boldsymbol{g}}{\partial \mathscr{U}}\frac{\partial \mathscr{U}}{\partial R} = -\frac{\partial \boldsymbol{g}}{\partial R}. \tag{3.23}$$

The linear system in (3.21) is solved by decomposing $\partial \boldsymbol{g}/\partial \mathscr{U}$ into triangular factors

$$\frac{\partial \boldsymbol{g}}{\partial \mathscr{U}} = \boldsymbol{PLUQ}, \tag{3.24}$$

where $\boldsymbol{P}$, $\boldsymbol{Q}$ are permutation matrices, and $\boldsymbol{L}$ and $\boldsymbol{U}$ are lower and upper triangular matrices respectively, and then solving two triangular systems. The $\boldsymbol{LU}$ decomposition is carried out by the frontal algorithm with a suitable pivoting procedure to maintain numerical stability (Duff 1981). Once the factors have been calculated, subsequent systems such as (3.23) may be solved relatively cheaply. One further benefit comes from this method of solution, namely the determinant of $\partial \boldsymbol{g}/\partial \mathscr{U}$ may be easily calculated as

$$\det\left(\frac{\partial \boldsymbol{g}}{\partial \mathscr{U}}\right) = \det(\boldsymbol{P})\det(\boldsymbol{L})\det(\boldsymbol{U})\det(\boldsymbol{Q}),$$

which is just the product of the pivots with appropriate changes of sign to account for row and column interchanges during the pivoting procedure. The sign of this determinant is, by definition, the index of the finite-dimensional problem which, for a sufficiently fine mesh, will agree with the Leray–Schauder index of the continuous problem (Lloyd 1978).

The Euler–Newton continuation procedure breaks down when a simple limit point is encountered, essentially because the parameter R is no longer suitable for parametrizing the branch of solutions. In this case we use the pseudo arclength continuation method due to Keller (1977). The basic idea is to parametrize the solution with an arclength-like parameter s, so that we look for $\mathscr{U}(s)$, $R(s)$ that satisfy

$$\boldsymbol{g}(\mathscr{U}, R) = 0, \tag{3.25}$$

$$N(\mathscr{U}, R, s) = 0, \tag{3.26}$$

where

$$N(\mathscr{U}, R, s) \equiv \frac{\partial \mathscr{U}}{\partial s}(s_0)^{\mathrm{T}}(\mathscr{U}(s)-\mathscr{U}(s_0)) + \frac{\partial R}{\partial s}(s_0)(R(s)-R(s_0)) - (s-s_0). \tag{3.27}$$

Euler–Newton continuation in s is applied to (3.25) and (3.26). The method works because the Jacobian matrix of the enlarged system

$$\begin{pmatrix} \dfrac{\partial \boldsymbol{g}}{\partial \mathscr{U}} & \dfrac{\partial \boldsymbol{g}}{\partial R} \\ \dfrac{\partial \mathscr{U}}{\partial s}(s_0)^{\mathrm{T}} & \dfrac{\partial R}{\partial s}(s_0) \end{pmatrix}$$

is non-singular, even at the simple limit point where $\partial \boldsymbol{g}/\partial \mathscr{U}$ is singular (Keller 1977). Keller also describes methods for switching branches at two-sided bifurcation points.

One method of solving two-parameter problems is to apply the above one-parameter method for a discrete set of values of the second parameter, and then to repeat the exercise with the roles of the two parameters reversed. This technique has been used by Keller & Szeto (1980) to study the problem of flow between rotating disks.

However, the structure of the solution surface is determined by the locus of bifurcation and limit points, and so it is only necessary to calculate these if a qualitative picture of the possible flows is required. This is the procedure we adopt in the present work. It is particularly appropriate here since the experimental results of Benjamin & Mullin (1981) are in precisely this form.

For fixed Γ, a set of equations that determine the symmetry-breaking bifurcation points in the Taylor problem is

$$\boldsymbol{g} + \Delta \boldsymbol{\psi} = 0, \tag{3.28}$$

$$\boldsymbol{\psi}^{\mathrm{T}} \frac{\partial \boldsymbol{g}}{\partial \mathscr{U}} = 0, \tag{3.29}$$

$$\boldsymbol{\psi}^{\mathrm{T}} \frac{\partial \boldsymbol{g}}{\partial R} = 0, \tag{3.30}$$

$$\boldsymbol{\psi}^{\mathrm{T}} \boldsymbol{\psi} = 1. \tag{3.31}$$

This extended system was introduced by Moore (1980), and he showed that Newton's method may be used to solve it for $\mathscr{U}, \boldsymbol{\psi}, R, \Delta$. The parameter Δ is introduced for numerical convenience, since otherwise the system would be overdetermined. If the discrete problem has a bifurcation, as in the present case, the Δ calculated will be zero to machine precision. We may write (3.28)–(3.31) in the form

$$\boldsymbol{F}(\mathscr{Y}, \Gamma) = 0, \tag{3.32}$$

where $\mathscr{Y} = (\mathscr{U}, \boldsymbol{\psi}, R, \Delta)$. Equation (3.32) can then be solved as a single-parameter problem in Γ, by continuation methods.

In order to calculate the simple limit points appearing in the Taylor problem, we use the following extended system:

$$\boldsymbol{g} = 0, \tag{3.33}$$

$$\frac{\partial \boldsymbol{g}}{\partial \mathscr{U}} \phi = 0, \tag{3.34}$$

$$l(\phi) = 1. \tag{3.35}$$

Equation (3.35) is simply a convenient normalization condition on the right eigenvector of $\partial \boldsymbol{g}/\partial \mathscr{U}$. Again this system may be solved by Newton's method (Moore & Spence 1980), and Euler–Newton continuation used to find the variation of the limit points with Γ.

4. Numerical results

The region D was divided up into quadrilateral elements. A typical mesh is shown in figure 2. The meshes used were uniform in the r- and z-directions with the exception of the elements in the corners next to the inner cylinder. Local refinement of the type shown in figure 2 was used. The purpose of this refinement was to model the rapid variation in the azimuthal velocity component between the inner cylinder and the ends of the cylinders. The grids may be characterized by the triple (NR, NZ, NC), where NR and NZ are the number of elements in the r- and z-directions respectively, and the grid has $2NC-1$ elements in each corner. The total number of degrees of freedom on such a grid is $3(2NR+1)(2NZ+1)+60(NC-1)+3NR \cdot NZ+12(NC-1)$ so that (5, 5, 5) and (10, 10, 5) grids have 726 and 1911 freedoms respectively. Note that $NC = 1$ implies the grid to be uniform. It was found that, provided NC was greater

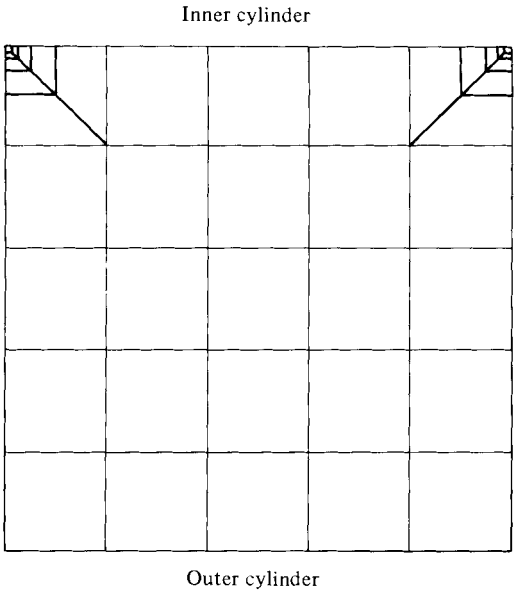

FIGURE 2. Typical finite-element grid of quadrilaterals used for the numerical calculations.

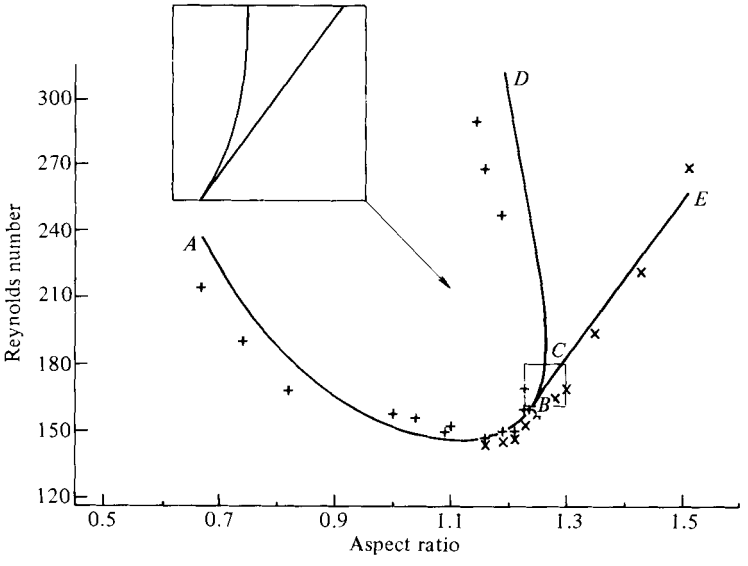

FIGURE 3. Critical loci for single-cell mode: ——, numerical predictions; +, experimental values for symmetry-breaking bifurcation points (from Benjamin & Mullin 1981); ×, experimental values for simple limit points (one-sided bifurcation points) (from Benjamin & Mullin 1981).

than about 4, further refinement only affected the flow close to the corners, and the critical Reynolds numbers were changed by a negligible amount.

The principal results of this paper are shown in figure 3. The curve $ABCD$ is the projection on the (R, Γ)-plane of the set of symmetry-breaking bifurcation points. The curve was produced by solving the Moore system (3.28)–(3.31) at about 20 different points along the curve. A cubic spline was fitted through the discrete values to give a continuous curve. All the points were calculated on the same (10, 10, 5) grid. The

Aspect ratio	Critical Reynolds number				Error in (10, 10, 5) grid results (%)
	$h = \frac{1}{5}$	$h = \frac{1}{7}$	$h = \frac{1}{10}$	$h = 0$ (extrapolated)	
0.67 (A)	252.3	240.1	237.3	236.4	0.4
1.00	156.8	152.7	152.1	151.9	0.1
1.187 (D)	261.5	299.0	313.2	317.7	1.4

TABLE 1. Variation of critical Reynolds number with grid size for three aspect ratios. Estimated error in (10, 10, 5) grid results is also shown.

error in the critical Reynolds number for a given aspect ratio is less than 0.5 % along AC and less than 1.5 % along CD. These errors were estimated using (3.19) and the results from (5, 5, 5), (7, 7, 5) and (10, 10, 5) grids. These values are given in table 1 for the most extreme points of the curve $ABCD$, where in fact the largest errors occur. The error along the curve near the minimum in critical Reynolds number is much smaller, being less than 0.2 %.

The curve BE is the projection on the (R, Γ)-plane of the set of simple limit points. The points along this curve were calculated using the Moore–Spence system (3.33)–(3.38) on a (7, 10, 5) grid at about 10 different values of Γ. The error along this curve is about 1 %. The aspect ratio corresponding to point B ($\Gamma = 1.235$) marks the onset of hysteresis.

Turning now to the experimental results (Benjamin & Mullin 1981), we see that there is good agreement along AB and BE between the experimental and numerically calculated points. The maximum discrepancy is less than 10 %, and along most of the curve it is less than 5 %. Along BD the agreement is not so good, the calculated values for the critical Reynolds numbers are about 30 % higher than the experimental values. These errors are probably due in part to the extreme steepness of the curve CD.

The range of aspect ratios over which hysteresis was observed in the experiments is 1.16–1.24, which differs significantly from the calculated range (1.235–1.265). The reason for this discrepancy is not obvious; however, the effect is a fairly delicate one and it is possible that the aspect ratio corresponding to the point B is very sensitive to small changes in the experimental apparatus. We feel that it is unlikely (unless there is some undetected error in the calculation) that further grid refinement would produce better agreement with the experiments since the aspect ratio at B was monotonic increasing as the grid was refined.

Figure 1 shows how the state diagram changes with aspect ratio in the range 1.23–1.27. These diagrams were calculated using Euler–Newton and Keller arclength continuation methods, described in §3, to obtain the solution at various values of the Reynolds number. A spline fit to the value of the vertical component of velocity at the point (0.75, 0) was used to produce the continuous curves shown in the diagrams. Note that this velocity is zero for a solution having class (i) symmetry. The integers associated with the various branches were calculated in the manner described in §3. No appropriate experimental results are available for comparison with figure 1, but the form of diagrams is precisely that predicted by Benjamin & Mullin (1981).

Finally, figure 4 shows the calculated streamline patterns for three distinct flows

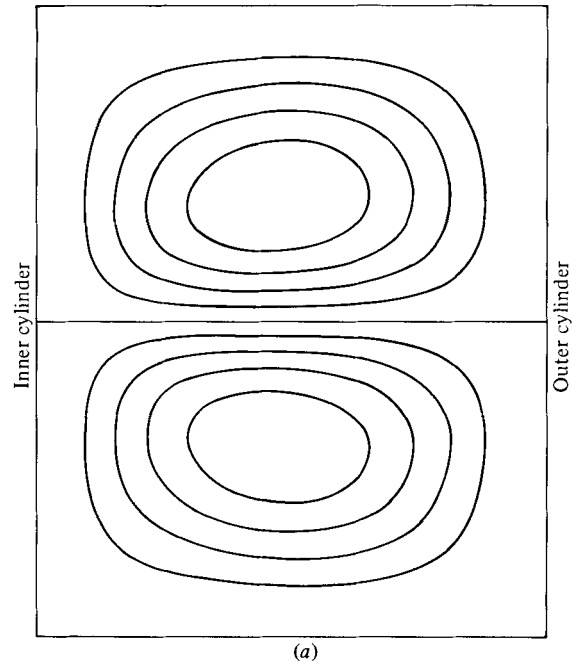

FIGURE 4. For caption see facing page.

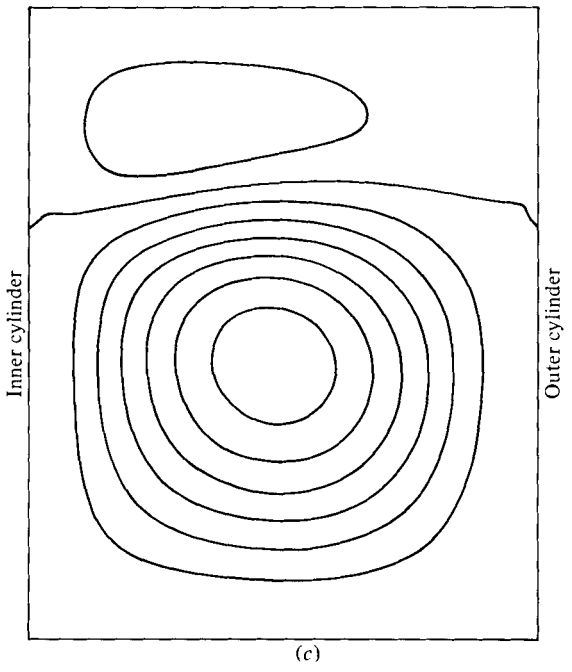

FIGURE 4. Streamline patterns for three distinct flows at Reynolds number 175 and aspect ratio 1.264. Equally spaced contours of the non-dimensional stream function are plotted. (*a*) Stable two-cell flow, (*b*) unstable asymmetric flow, (*c*) stable 'single-cell' flow.

with aspect ratio 1.264 and Reynolds number 175. Figure 4(*a*) is the stable two-cell flow and 4(*c*) is the stable single-cell flow. It is interesting to note that there are in fact two cells here, although the upper cell is very weak and in an experimental observation probably appears as a region of stagnant fluid. Figure 4(*b*) shows the asymmetric unstable flow which lies on the subcritical branch coming from the bifurcation of the two-cell flow (cf. figure 1*c*). This flow is not observable experimentally, of course, and it is interesting that its asymmetry is much less marked than that of the stable flow in figure 4(*c*). The reflections in the plane $z = 0$ of the flows in figures 4(*b*, *c*) are also possible flows, though they are not shown here.

5. Conclusions

We have applied various numerical methods for solving nonlinear equations and bifurcation problems to a finite-element discretization of steady axisymmetric flow in the Taylor problem with realistic end conditions. The methods, though comparatively recent, are now standard means of solving bifurcation problems numerically. Their application to the Taylor problem is new as far as is known and they have proved capable of giving both a qualitative and quantitative picture of the solution to the problem. Some of the effects examined, particularly the hysteresis effects, are extremely delicate but posed no great problem for the numerical methods employed. Recently Benjamin & Mullin (1982) speculated that profuse multiplicity in the Taylor problem is liable to complicate a numerical approach. While this statement is not disputed a tentative conclusion to be drawn from the present work is that methods similar to those employed here are powerful enough to resolve the complications and

give a complete description of the steady axisymmetric flows possible in the Taylor experiment for moderate aspect ratio. It should be emphasized, however, that such an exercise is likely to need significant computer resources and the methods would not be suitable for attacking the general problem where unsteady non-axisymmetric flows must be considered.

The numerical results obtained in this paper are in quite satisfactory quantitative agreement with those obtained by Benjamin & Mullin (1981) and, perhaps most significantly, the qualitative behaviour of the flow is confirmed to be precisely as proposed by Benjamin & Mullin (1981).

The author is grateful to Dr T. Mullin for providing the experimental data used in figure 3 in tabulated form.

REFERENCES

BENJAMIN, T. B. 1976 Application of Leray–Schauder degree theory to problems of hydrodynamic stability. *Math. Proc. Camb. Phil. Soc.* **79**, 373–392.

BENJAMIN, T. B. 1978*a* Bifurcation phenomena in steady flows of a viscous liquid. I. Theory. *Proc. R. Soc. Lond.* A **359**, 1–26.

BENJAMIN, T. B. 1978*b* Bifurcation phenomena in steady flows of a viscous liquid. II. Experiments. *Proc. R. Soc. Lond.* A **359**, 27–43.

BENJAMIN, T. B. 1978*c* Applications of generic bifurcation theory in fluid mechanics. In *Contemporary Developments in Continuum Mechanics and Partial Differential Equations* (ed. G. M. de la Penha & L. A. J. Madeiros). Mathematical Studies **30**. North-Holland.

BENJAMIN, T. B. & MULLIN, T. 1981 Anomalous modes in the Taylor experiment. *Proc. R. Soc. Lond.* A **377**, 221–249.

BENJAMIN, T. B. & MULLIN, T. 1982 Notes on the multiplicity of flows in the Taylor experiment. *J. Fluid Mech.* **121**, 219–230.

BREZZI, F., RAPPAZ, J. & RAVIART, P. A. 1980 Finite dimensional approximation of nonlinear problems. I. Branches of nonsingular solutions. *Numer. Math.* **36**, 1–25.

BREZZI, F., RAPPAZ, J. & RAVIART, P. A. 1981*a* Finite dimensional approximation of nonlinear problems. II. Limit points. *Numer. Math.* **37**, 1–28.

BREZZI, F., RAPPAZ, J. & RAVIART, P. A. 1981*b* Finite dimensional approximation of nonlinear problems. III. Simple bifurcation points. *Numer. Math.* **38**, 1–30.

CLIFFE, K. A., JACKSON, C. P. & GREENFIELD, A. C. 1982 Finite-element solutions for flow in a symmetric channel with a smooth expansion. *Harwell Rep.* AERE R-10608. HMSO.

DIPRIMA, R. C. 1981 Transition in flow between rotating concentric cylinders. In *Transition and Turbulence* (ed. R. E. Meyer), pp. 1–23. Academic.

DUFF, I. S. 1981 MA32 – A package for solving sparse unsymmetric systems using the frontal method. *Harwell Rep.* AERE R-10079. HMSO.

ENGLEMAN, M. S., SANI, R. L., GRESHO, P. M. & BERCOVIER, M. 1982 Consistent vs. reduced integration penalty methods for incompressible media using several old and new elements. *Intl J. Numer. Methods Fluids* **2**, 25–42.

FOIAS, C. & TEMAM, R. 1977 Structure of the set of stationary solutions of the Navier–Stokes equations. *Commun. Pure Appl. Maths* **30**, 149–164.

GIRAULT, V. & RAVIART, P. A. 1979 *Finite Element Approximation of the Navier–Stokes Equations.* Lecture Notes in Mathematics, vol. 749. Springer.

KELLER, H. B. 1977 Numerical solutions of bifurcation and nonlinear eigenvalue problems. In *Applications of Bifurcation Theory* (ed. P. H. Rabinowitz), pp. 359–384. Academic.

KELLER, H. B. & SZETO, R. K. H. 1980 Calculation of flows between rotating disks. In *Computing Methods in Applied Science and Engineering* (ed. R. Glowinski and J. L. Lions), pp. 51–61. North-Holland.

LADYZHENSKAYA, O. A. 1969 *The Mathematical Theory of Viscous Incompressible Flow*, 2nd edn. Gordon & Breach.

LLOYD, N. G. 1978 *Degree Theory*. Cambridge University Press.

MOORE, G. 1980 The numerical treatment of nontrivial bifurcation points. *Numer. Funct. Anal. and Optimiz.* **2**, 441–472.

MOORE, G. & SPENCE, A. 1980 The calculation of turning points of nonlinear equations. *SIAM J. Numer. Anal.* **17**, 567–576.

MULLIN, T. 1982 Mutations of steady cellular flows in the Taylor experiment. *J. Fluid Mech.* **121**, 207–218.

SCHAEFFER, D. G. 1980 Analysis of a model in the Taylor problem. *Math. Proc. Camb. Phil. Soc.* **87**, 307–337.

SERRIN, J. 1959 On the stability of viscous fluid motions. *Arch. Rat. Mech. Anal.* **3**, 1–13.

WERNER, B. & SPENCE, A. 1983 The computation of symmetry-breaking bifurcation points. *SIAM J. Numer. Anal.* (To appear).